Received: 9 October 2024 | Revised: 7 March 2025 | Accepted: 21 April 2025

DOI: 10.1002/qj.5014

Quarterly Journal of the Royal Meteorological Society RMetS

RESEARCH ARTICLE

Convection-permitting dynamical downscaling of ERA5 for Europe and the Mediterranean basin

Lisa Bernini[1,2] | **Martina Lagasio**[2] | **Massimo Milelli**[2] | **Elena Oberto**[2] | **Antonio Parodi**[2] | **Stephan Hachinger**[3] | **Dieter Kranzlmüller**[3,4] | **Nazario Tartaglione**[5]

[1]University of Genoa, Genoa, Italy

[2]CIMA Research Foundation, Savona, Italy

[3]Leibniz Supercomputing Centre (LRZ) of the Bavarian Academy of Sciences and Humanities, Garching, Germany

[4]Ludwig-Maximilians-Universität München, Munich, Germany

[5]Italian Institute for Environmental Protection and Research, Rome, Italy

Correspondence
Lisa Bernini, CIMA Foundation, Savona, 17100, Italy.
Email: lisa.bernini@cimafoundation.org

Funding information
I-CHANGE (Individual Change of HAbits Needed for Green European transition), Grant/Award Number: 101037193; TRIGGER (SoluTions foR mItiGatinG climate-induced hEalth thReats), Grant/Award Number: 101057739

Abstract

As the European continent and the Mediterranean Sea experience rapid warming trends and diverse manifestations of extreme weather, there is an urgent need to understand and mitigate the impacts of climate change in these regions. This study introduces the Computational Hydrometeorology with Advanced Performance to Enhanced Realism (CHAPTER) high-resolution dynamical downscaling of the European Centre for Medium-Range Weather Forecasts Reanalysis v5 (ERA5) global reanalysis made with the Weather Research and Forecasting numerical model. CHAPTER covers Europe and the Mediterranean basin at a convection-resolving grid resolution of 3 km by 3 km. CHAPTER's performances in representing precipitation and temperature are evaluated compared to state-of-the-art datasets like ERA5-Land. The focus is put on seasonal spatial distributions of the bias and the root mean square error, and fuzzy verification techniques are used to validate the precipitation outputs. The results reveal that CHAPTER's performance aligns closely with well-recognized downscalings of ERA5 but has, in addition, the advantage of providing a rich portfolio of variables at hourly temporal resolution and on different terrain, following model levels. Therefore, CHAPTER is a valuable resource for studying extreme weather events, offering insights crucial for climate change adaptation and mitigation efforts in Europe and the Mediterranean region.

KEYWORDS

convection-permitting, downscaling, ERA5, hindcast, WRF

1 | INTRODUCTION

The increasing frequency and severity of extreme weather events with global warming (Diffenbaugh *et al.*, 2017) pose significant challenges to societies worldwide, amplifying concerns about the resilience of infrastructure and ecosystems in the face of climate change (Calleja-Agius *et al.*, 2021; Cramer *et al.*, 2018). As global warming accelerates, the manifestations of extreme weather, from intense precipitation to prolonged heat waves, are becoming

more pronounced, affecting diverse regions with varying impacts. Europe, in particular, is experiencing rapid warming trends, outpacing many other parts of the globe. Over the past decade, according to Canadell *et al.* (2021), the average land temperature in Europe has surged by 2.10°C compared with pre-industrial levels, surpassing the global average rise of 1.17°C. This disparity in temperature increase underscores the urgency of understanding and mitigating the impacts of climate change, especially in vulnerable regions of Europe, such as the densely populated Mediterranean basin, mountainous terrains, and coastal areas.

Extreme weather events, including heatwaves, droughts, floods, and storms, have already inflicted substantial economic losses, public health crises, and environmental degradation across Europe (Bakkensen, 2017; Weilnhammer *et al.*, 2021). Southern and central Europe are witnessing heightened occurrences of heatwaves (Rahmstorf & Coumou, 2011; Schär *et al.*, 2004), forest fires (Moriondo *et al.*, 2006), and droughts (Grillakis, 2019), whereas northern and northeastern regions face increased risks of heavy precipitation (Hosseinzadehtalaei *et al.*, 2020; Vautard *et al.*, 2014), flooding (Alfieri *et al.*, 2015; Hendry *et al.*, 2019), and coastal erosion. The consequences of these events extend beyond immediate damage, impacting sectors ranging from agriculture and energy (Bonanno *et al.*, 2019) to public health and transportation.

In response to the escalating challenges posed by extreme weather, there is a growing imperative to enhance our understanding of these phenomena through advanced modeling and analysis techniques (Apicella *et al.*, 2021; Fiori *et al.*, 2017; Rossa *et al.*, 2011; Vié *et al.*, 2012). One promising approach is the development and utilization of convection-permitting regional climate models (CP-RCMs), which offer unprecedented spatial resolution (typically inferior to 4 km) and enable detailed simulations of local-scale weather processes (Kendon *et al.*, 2021). Recent advancements in CP-RCMs have shown promising results in capturing the characteristics of extreme precipitation events, diurnal variability, spatial distribution, and intensity gradients with improved fidelity compared with traditional climate models (Lucas-Picher *et al.*, 2021; Pieri *et al.*, 2015; Prein *et al.*, 2015). Moreover, CP-RCMs exhibit enhanced capabilities in detecting surface heterogeneities (Ntagkounakis *et al.*, 2023), such as mountains (Dalla Torre *et al.*, 2024), coastal regions (Vannucchi *et al.*, 2021), and urban areas (Reder *et al.*, 2022), and accurately representing land–atmosphere interactions crucial for understanding and predicting extreme weather phenomena (Coppola *et al.*, 2020; Karki *et al.*, 2017).

In parallel, the advent of high-resolution climate reanalysis datasets has revolutionized our ability to reconstruct past weather conditions and monitor ongoing climate trends. By assimilating historical observations from diverse sources, these reanalysis products provide a comprehensive and consistent depiction of the atmospheric state, facilitating a deeper understanding of weather-related phenomena (Trenberth *et al.*, 2008). Notably, the European Centre for Medium-Range Weather Forecasts (ECMWF) has released ECMWF Reanalysis v5 (ERA5), a global reanalysis dataset offering unprecedented spatial and temporal resolution (Hersbach *et al.*, 2020). In the present study, a dynamical downscaling of the ERA5 global reanalysis (31 km × 31 km grid) has been used. This downscaling, called Computational Hydrometeorology with Advanced Performance to Enhanced Realism (CHAPTER), has been made with the mesoscale numerical weather prediction model Advanced Research Weather Research and Forecasting (WRF; Skamarock *et al.*, 2008) over Europe and the Mediterranean region on a grid of 3 km × 3 km from 1981 to 2022.

The availability of these meteorological fields at such high-spatial temporal resolution over the European continental scale is, to our best knowledge, currently unique in international climatological research. Different subcontinental reanalyses exist, such as the European CORDEX domain (Coordinated Regional Downscaling Experiment, https://cordex.org), COSMO-REA6 (Bollmeyer *et al.*, 2015), the HIRLAM-based reanalysis (Dahlgren *et al.*, 2016), the Copernicus European Regional Reanalysis datasets (Ridal *et al.*, 2024; Schimanke *et al.*, 2021), and MERIDA covering the Italian peninsula (Bonanno *et al.*, 2019). However, convection remains parametrized in these regional reanalyses due to the significant computational expenses associated with generating datasets at kilometer-scale grid resolution, especially for extensive domains. Convection-permitting resolution has thus far been attained solely for national or even smaller geographic areas. For example, MERA (Met Eireann Reanalysis) covers Ireland and the United Kingdom with a horizontal resolution of 2.5 km (Gleeson *et al.*, 2017), COSMO-REA2, a 2 km resolution dataset, covers central Europe (Wahl *et al.*, 2017), and, finally, SPHERA (Cerenzia *et al.*, 2022; Giordani *et al.*, 2023) and VHR-REA-IT (Raffa *et al.*, 2021) are two high-resolution downscalings of ERA5 at a 2.2 km grid-scale level, but only for Italy.

The domain of CHAPTER spans from the Atlantic Ocean to the Black Sea and from the Sahara Desert to the southern regions of Scandinavia. With a dataset covering 42 years of data terrain-following model levels, CHAPTER offers a comprehensive resource for investigating the evolution, drivers, and impacts of extreme weather events at both local and regional scales over the past decades. Subsequent sections provide an overview of the model

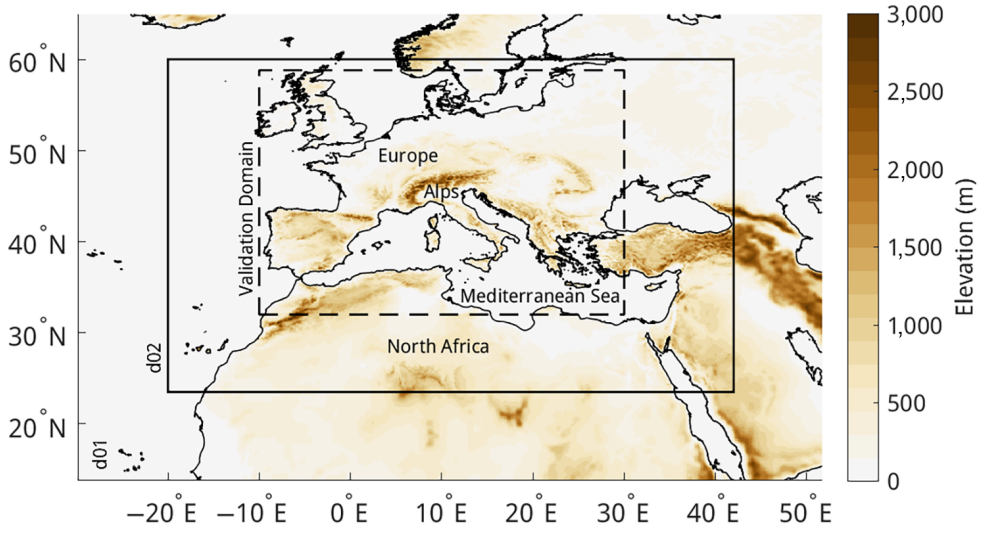

FIGURE 1 Domain of the CHAPTER dataset with a resolution of 3 km by 3 km (entire graph) and domain used for the validation (internal black rectangle) [Colour figure can be viewed at wileyonlinelibrary.com]

configuration and an assessment of CHAPTER's performance in accurately representing precipitation and temperature compared with state-of-the-art datasets.

2 | MATERIALS AND METHODS

2.1 | Model configuration

The downscaling was performed using the WRF numerical model, with ERA5 data used as initial and boundary conditions. ERA5 is a state-of-the-art global climate reanalysis dataset developed by ECMWF as part of the Copernicus Climate Change Service. This dataset represents the fifth generation of ECMWF reanalysis products, succeeding ERA-Interim. ERA5 offers significant advancements over its predecessor, ERA-Interim, boasting higher spatial and temporal resolutions, with grid resolutions of approximately 31 km and temporal resolutions of 1 hr. It incorporates a wealth of observational data, including ozone-sensitive infrared radiance and reprocessed datasets not utilized in previous versions. The data assimilation system of ERA5 is based on Cycle 41r2 of the Integrated Forecast System, operating within 12-hr time windows. Released in 2017, ERA5 provides comprehensive coverage from 1940 to the present, continuously updated with a 2-month delay.

ERA5 data were retrieved with an hourly temporal resolution for CHAPTER computation to assure good temporal consistency. They served as initial and boundary conditions for the model runs. The computational domains consist of two grids with a horizontal resolution of 9 km (30°W–52°E, 14°N–65°N, $716 \times 634 \times 50$ grid points) and 3 km (20°W–42°E, 23.5°N–60°N, $1{,}640 \times 1{,}352 \times 50$ grid points), respectively (Figure 1). For each day, the WRF run is initialized at 1800 UTC and covers the following 30 hr. Each new run is initialized after 30 hr from the initial condition given by ERA5, and the first 6 hr are considered as spin-up time and thus discarded. Hence, each run is connected to the following one at 0000 UTC and all the runs are independent of each other. Having a run starting from ERA5's initial conditions each day prevents the dataset from deviating too much from the large-scale atmospheric condition of ERA5 and explains why no spectral nudging was used.

The WRF version used is 4.1.1. The model physical set-up is derived to a large extent from the Pieri *et al.* (2015) and von Hardenberg *et al.* (2015) studies with finer grid spacing (from 4 km to 3 km), very well suited for severe weather phenomena dynamical downscaling, and covers a significantly larger area than those previous studies. In particular, the Yonsei University scheme (Hong *et al.*, 2006) is chosen for the planetary boundary layer turbulence closure; the Rapid Radiative Transfer Model for GCMs short-wave and long-wave schemes are used for radiation (Iacono *et al.*, 2000, 2008; Mlawer *et al.*, 1997); and the Rapid Update Cycle scheme is chosen as a multilevel soil model (six levels) with higher resolution in the upper soil layer: 0, 5, 20, 40, 160, and 300 cm (Smirnova *et al.*, 1997, 2000). No cumulus scheme was activated in the innermost domains (d02) because the grid spacing allows the convection dynamics to be resolved. The convection scheme used in the outer domain (d01) is the New Simplified Arakawa–Schubert scheme (Han & Pan, 2011), which is a mass flux scheme based on Pan (1995) with revisions made to the entrainment and detrainment formulation following large-eddy simulation studies. The deep convection was made stronger by increasing the maximum allowable mass flux at the cloud base.

2.2 | Validation

2.2.1 | Observations datasets and comparative downscalings

The performances of CHAPTER have been evaluated on 24-hr precipitation accumulation and 2-m daily mean temperature. They are compared with the performance of the ERA5-Land reanalysis (Muñoz-Sabater *et al.*, 2021) and with the high-resolution precipitation dataset CHELSA (Karger *et al.*, 2021). The observation datasets used to confront the models' outputs are E-OBS (Cornes *et al.*, 2018), both for temperature and precipitation, and EURADCLIM (Overeem *et al.*, 2022), only for precipitation. A description of each dataset is provided hereafter. All the datasets are publicly available.

ERA5-Land is a refinement of ERA5, achieved through a process of physical downscaling. It utilizes high-resolution global numerical integration of the ECMWF land-surface model, driven by meteorological data downscaled from ERA5 climate reanalysis. Notably, an elevation correction is applied to enhance the accuracy of near-surface thermodynamic conditions. Though inheriting most parametrizations from ERA5, ERA5-Land distinguishes itself with a significantly improved horizontal resolution of ∼10 km ($0.1° \times 0.1°$) compared with ERA5's 31 km. Both datasets maintain an hourly temporal resolution. Evaluations against various independent datasets demonstrate ERA5-Land's performance in depicting the hydrological cycle (Wu *et al.*, 2023).

CHELSA utilizes a statistical downscaling approach to enhance the resolution of daily precipitation estimates. This method integrates high-resolution satellite-derived cloud frequency data (30″, approximately 1 km) with orographic predictors such as wind fields, valley exposition, and boundary layer height. The downscaling process involves bias correction to refine the results. By applying this approach to the ERA5 precipitation archive and MODIS monthly cloud cover frequency, a daily gridded precipitation time series in 1 km resolution from 2003 to 2016 is generated. Comparative analyses with existing datasets and station data, the Global Historical Climatology Network daily (Menne *et al.*, 2012), reveal improved spatio-temporal performance in precipitation prediction.

E-OBS is a daily gridded land-only observational dataset covering Europe at a horizontal resolution of 0.1° (∼ 10 km), sourced from the European Climate Assessment & Dataset project. This dataset includes precipitation amount, temperature, relative humidity, sea-level pressure, and surface short-wave downwelling radiation. Initially developed for model validation, E-OBS is now widely used for climate monitoring, offering a unique combination of spatial resolution, daily resolution, and multiple variables. Though valuable for climate research, E-OBS has limitations (Hofstra *et al.*, 2009), including potential underestimations in precipitation and systematic errors, especially for convective rainfall. In addition, the dataset's reliance on station data with varying densities across countries and variations in the 24-hr observation period highlights the need for careful interpretation (Bandhauer *et al.*, 2022).

Finally, EURADCLIM, the European climatological gauge-adjusted radar precipitation dataset, offers high-resolution (sub-)daily precipitation data covering 8,000,000 km^2 of Europe. It provides 1-hr and 24-hr accumulations at a 2-km grid from 2013 to 2020 and is updated every year. Beginning with the EUMETNET OPERA gridded radar dataset, EURADCLIM employs methods to filter non-meteorological echoes and merges the radar composites with rain-gauge data from the European Climate Assessment & Dataset, significantly enhancing its quality (Overeem *et al.*, 2022).

2.2.2 | Validation techniques

A fuzzy verification approach, as described by Ebert (2008), is utilized to compare the precipitation performances of CHAPTER, CHELSA, and ERA5-Land. Unlike traditional nearest-point verifications, which seek exact matches between forecast and observation pairs, fuzzy verification methods relax matching conditions between the model and observations. In this approach, forecasts are required to be in approximate agreement with observations, considering factors such as proximity in space, time, or other quantities. This is particularly beneficial for high-resolution models, where matching observations with absolute precision is challenging, as it mitigates "double-penalty" issues (Rossa *et al.*, 2008), where correct forecasting may still be penalized for being offset from observations. Moreover, owing to the sparse nature of rain-gauge observations, a spatial aggregation is necessary to objectively assess the quality of model simulations and compensate for representativeness limitations that affect individual point observations.

This study adopted the "anywhere-in-the-window" fuzzy verification approach, as described by (Ebert, 2008). This is a special case of the "minimum coverage" technique, an example of the neighborhood observation–neighborhood forecast strategy. In particular, the fraction skill score (FSS) serves as a primary index summarizing the potential of fuzzy verification logic, comparing forecast and observation fields within defined event areas. It is

given by

$$\mathrm{FSS} = 1 - \frac{\frac{1}{N}\sum_{i=1}^{N}(P_{\mathrm{mod},i} - P_{\mathrm{obs},i})^2}{\frac{1}{N}\sum_{i=1}^{N}P_{\mathrm{mod},i}^2 + \frac{1}{N}\sum_{i=1}^{N}P_{\mathrm{obs},i}^2}, \quad (1)$$

with N the number of verification boxes in the domain under study and P the fraction of every single box in which the event occurs (the subscripts "mod" and "obs" stand for "forecast" and "observed" respectively). The FSS ranges from 0 (complete disagreement) to 1 (perfect agreement). FSS = 0 if there are no expected events but they do occur; or, vice versa, if no events that have been foreseen do occur.

The FSS value above which the forecast is considered useful (better than the random data) is given by $\mathrm{FSS}_{\mathrm{useful}} = 0.5 + (f_0/2)$, where f_0 is the fraction of the domain covered by the observed event (Roberts & Lean, 2008). The smallest spatial window for which $\mathrm{FSS} \geq \mathrm{FSS}_{\mathrm{useful}}$ is considered to be the useful scale. As the dimensions of the spatial windows increase, the index tends asymptotically to a value between 0 and 1. The closer this value is to 1, the less biased the forecast is.

Two other complementary scores are considered in our fuzzy verification approach: the false alarm ratio (FAR) and the probability of detection (POD). The FAR indicates the rate at which false detection occurs (range: 0–1; perfect value: 0). It is calculated as

$$\mathrm{FAR} = \frac{\text{false alarms}}{\text{hits} + \text{false alarms}}. \quad (2)$$

The POD, on the other hand, is the rate at which real events are successfully detected (range: 0–1; perfect value: 1). It is given by

$$\mathrm{POD} = \frac{\text{hits}}{\text{hits} + \text{misses}}. \quad (3)$$

For precipitation, a last score is also computed but not following a fuzzy approach; namely, the percentage bias, defined as

$$\text{Percentage bias} = \frac{1}{N}\sum_{n=1}^{N}\frac{M_i - O_i}{O_i} \times 100, \quad (4)$$

with N the size of the sample data, M_i the model predictions, and O_i the observations.

To compare the scores obtained by CHAPTER and CHELSA with respect to the EURADCLIM dataset (Figures 6 and 7), CHAPTER, CHELSA, and EURADCLIM have been regridded thanks to a nearest-neighbor remapping to a 3 km by 3 km regular grid. Because of the available period in EURADCLIM and CHELSA, this first comparison is made taking only into account the years from 2013 to 2016. In the same way, to obtain the scores by CHAPTER, CHELSA, and ERA5-Land computed with respect to E-OBS, all datasets have been regridded to a 10 km by 10 km regular grid. For those datasets, the available period is from 2003 to 2016. Finally, for both analyses, to take into account the different spatial coverage, the validation domain retained is 10°W–30°E; 32°N– 58.8°N (401 × 269 grid points; Figure 1).

TABLE 1 Mean bias of daily mean temperature of CHAPTER upscaled at 10 km and ERA5-Land temperatures for each season over all the domain (1981–2022).

	Mean bias (°C)	
	CHAPTER	**ERA5-Land**
Spring	0.02 (0.01)	0.21 (0.01)
Summer	0.55 (0.01)	0.70 (0.01)
Autumn	−0.02 (0.01)	0.45 (0.01)
Winter	−0.67 (0.01)	−0.04 (0.01)

The same validation domain is used for temperature. Temperature fields have been validated by comparing the bias (or mean error) and the root-mean-square error (RMSE) obtained by CHAPTER and ERA5-Land respectively with E-OBS daily temperature:

$$\mathrm{Bias} = \frac{1}{N}\sum_{n=1}^{N}M_i - O_i, \quad (5)$$

$$\mathrm{RMSE} = \sqrt{\frac{1}{N}\sum_{n=1}^{N}(M_i - O_i)^2}, \quad (6)$$

still with N the size of the sample data, M_i the model predictions, and O_i the observations.

Again, the data of CHAPTER, ERA5-Land, and E-OBS have been regridded on the same 10 km by 10 km regular grid. For temperature, a correction with a constant lapse rate of 6.5 $\mathrm{K} \cdot \mathrm{km}^{-1}$ has been applied to account for the differences in the elevation grid cells of the different datasets.

The seasonal means of the bias and the RMSE have been computed at each grid point and over the entire domain. A bootstrap technique (Efron, 1992) has been adopted to estimate the error of the global seasonal means. Each seasonal mean of the bias and the RMSE has been recomputed 1,000 times each time, taking into account only 5% of all the data. The differences between the 97.5th percentile and the 2.5th percentile of this distribution of means, the boundaries of the 95% confidence interval, are the final errors present in Tables 1 and 2.

Finally, for both temperature and precipitation we computed the added value (AV) as defined in

TABLE 2 Mean root-mean-square error (RMSE) of the daily mean temperature of CHAPTER upscaled at 10 km and ERA5-Land temperatures for each season over the entire domain (1981–2022).

	Mean RMSE (°C)	
	CHAPTER	**ERA5-Land**
Spring	1.80 (0.02)	1.64 (0.02)
Summer	2.02 (0.02)	2.04 (0.02)
Autumn	1.66 (0.01)	1.60 (0.01)
Winter	2.18 (0.02)	1.72 (0.01)

Dosio *et al.* (2015) (range: −1 to +1; perfect value: 1):

$$\mathrm{AV} = \frac{(X_{\mathrm{ERA5}} - X_{\mathrm{E\text{-}OBS}})^2 - (X_{\mathrm{CHAPTER}} - X_{\mathrm{E\text{-}OBS}})^2}{Max((X_{\mathrm{ERA5}} - X_{\mathrm{E\text{-}OBS}})^2, (X_{\mathrm{CHAPTER}} - X_{\mathrm{E\text{-}OBS}})^2)}, \quad (7)$$

with X the spatial distribution of the variable considered.

The AV is a way of assessing where CHAPTER shows improvement over ERA5, taking E-OBS as the ground truth. Over the points where the AV is negative, ERA5 is more in agreement with E-OBS than CHAPTER. In contrast, over the points where the AV is positive, CHAPTER has generated added value in comparison with ERA5. For this last analysis, both E-OBS and CHAPTER have been upscaled at the resolution of ERA5, 31 km by 31 km.

3 | RESULTS

3.1 | Precipitation

3.1.1 | Bias

Figure 2 presents the seasonal spatial distribution of the percentage bias of precipitation accumulation at 24 hr of ERA5-Land and CHAPTER enhanced on a 10 km by 10 km grid assuming E-OBS as reference. With respect to ERA5, CHAPTER has a higher positive bias, especially in summer over continental Europe. It is known that WRF simulations show a systematic positive precipitation bias and an overestimation of wet-day frequency (Warrach-Sagi *et al.*, 2013). In terms of spatial distribution, both datasets underestimate the precipitation over the African coast of the Mediterranean region, whereas the Alps are the main region where precipitation is overestimated. In both regions, underestimation and overestimation are partially due to the low density of the E-OBS network.

3.1.2 | Fuzzy verification scores

To have a more comprehensive view of the model's capability to represent precipitation fields, we analyzed the FSS, FAR, and POD scores, where a good performance corresponds to high FSS and POD values but low FAR values. In particular, the indices are shown as functions of spatial scale (abscissas) and precipitation threshold (ordinates); namely, the dimension of the side of the verification box. In this way, by looking at the lower right corner of these charts, it is possible to assess the model performances for events characterized by small spatial scales and high intensity, which are of primary importance in developing strong convective events.

Therefore, eight thresholds of precipitation intensities are considered; namely, 0.5, 1.0, 2.0, 5.0, 8.0, 12.0, 16.0, and 20.0 mm · day^{-1}. The agreements between the models and the observations are evaluated starting from a single grid pixel (i.e., 3 km by 3 km cells for the comparisons with the EURADCLIM dataset and 10 km by 10 km cells for the comparisons with the E-OBS dataset) up to squares with 11 pixels (i.e., 33 km by 33 km cells for the comparisons with

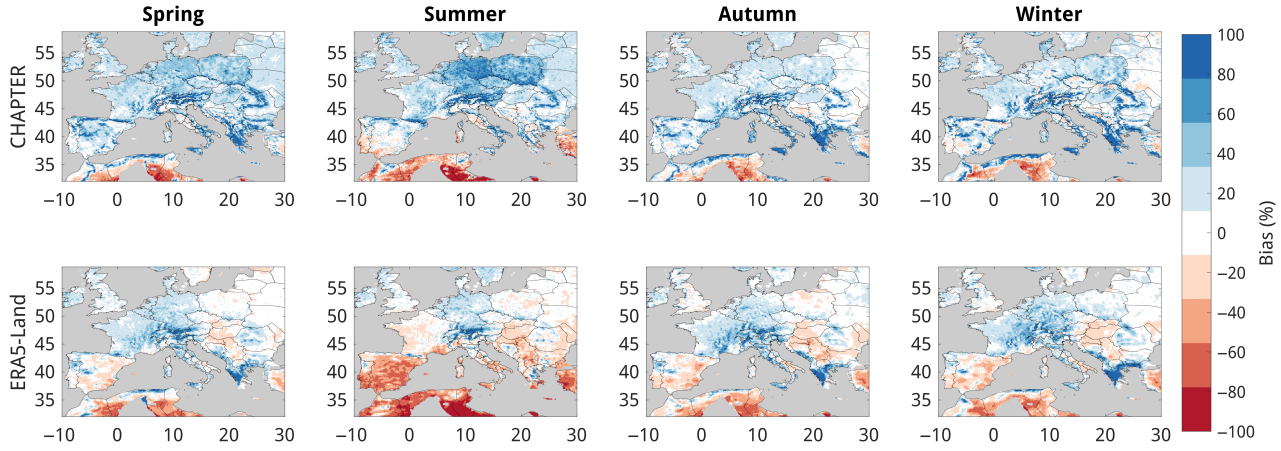

FIGURE 2 Percentage bias of the daily precipitation accumulation of CHAPTER (top) at 10 km and ERA5-Land (bottom) compared to E-OBS for the period 1981–2022. [Colour figure can be viewed at wileyonlinelibrary.com]

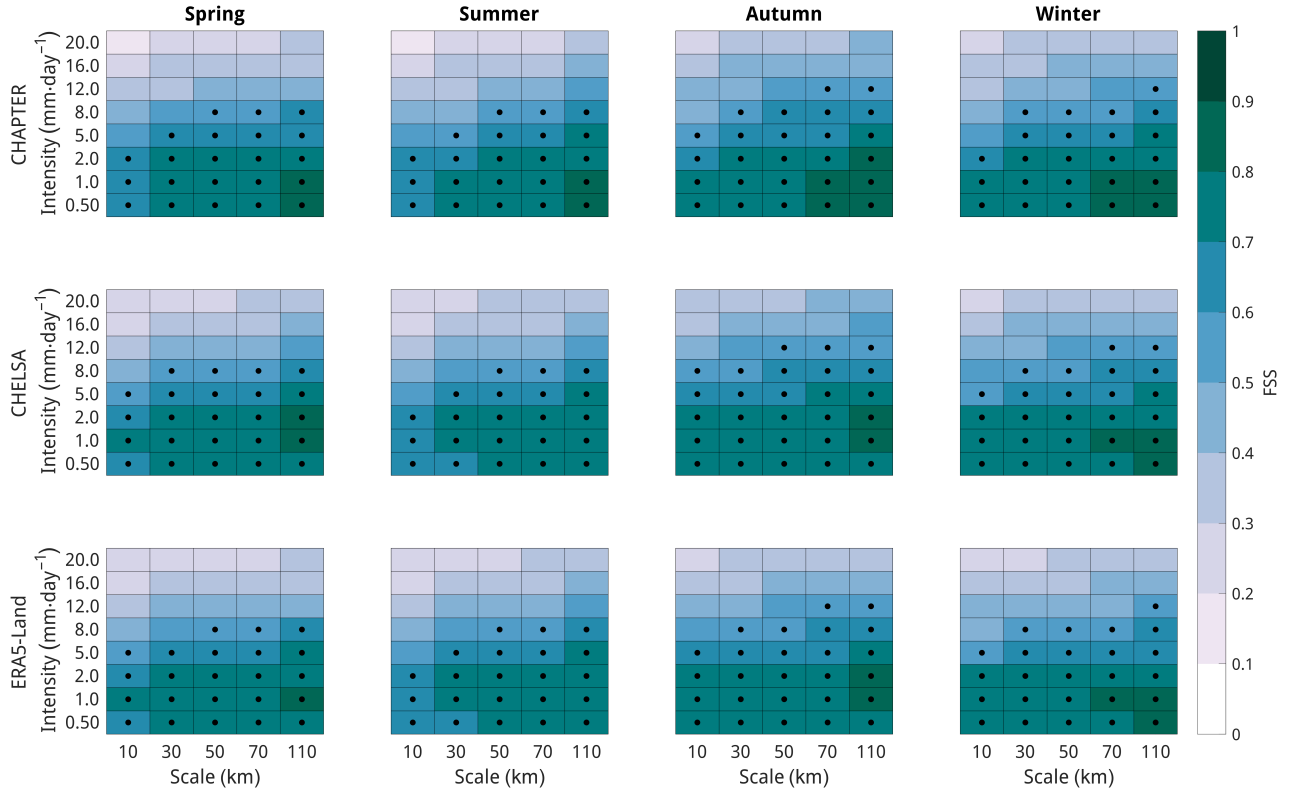

FIGURE 3 Fraction skill score (FSS) of the daily precipitation accumulation of CHAPTER (top) and CHELSA (center) at 10 km, and ERA5-Land (bottom) against E-OBS for the period 2003–2016. Black dots denote useful FSS values. [Colour figure can be viewed at wileyonlinelibrary.com]

the EURADCLIM dataset and 110 km by 110 km cells for the comparisons with the E-OBS dataset).

For the comparison between the upscaled version of CHAPTER and CHELSA, and ERA5-Land, with E-OBS, considered as the ground truth, all datasets have better performance in autumn and winter. Both FSS scores (Figure 3) and POD scores (Figure 5) are high and the FAR scores (Figure 4) are low, meaning true events are correctly represented and the ratio of non-existing events is low. For autumn and winter, the models are reliable for a spatial scale of 30 km and an intensity of 8 mm · day^{-1}, as indicated by the dots in Figure 3. The worst scores, however, are found in summer, where the FSS and POD scores are low and the frequency of false detection increases. In summer, the reliable intensity decreases to 5 mm · day^{-1} for a spatial scale of 30 km, meaning that strong localized convective events are not well represented.

CHAPTER performs very similarly to the two other datasets. Some differences can however be observed. In spring, for CHAPTER, the intensity of 5 mm · day^{-1} at a scale of 10 km cannot be considered reliable, whereas it is for the other datasets. As already mentioned, the FAR scores also indicate that CHAPTER overestimates the strongest intensities ($\geq$ 16 mm · day^{-1}) in spring and summer for every scale (Figure 4). The high FAR scores at these scales are associated with higher POD scores for CHAPTER than for the other two datasets (Figure 5). It shows that, in general, CHAPTER represents more strong convective events, increasing both probabilities of capturing events observed in E-OBS and events not present in the observation dataset.

Focusing on the comparison between CHAPTER and CHELSA with EURADCLIM at the native resolution of CHAPTER (3 km; Figures 6–8) confirms our conclusions: CHAPTER can be reliable up to a scale of 10 km for precipitation intensities of 5 mm · day^{-1} or 30 km for intensities of 8 mm · day^{-1}. The main difference with CHELSA is in summer at a scale of 3 km, where CHAPTER is not reliable for any of the intensities. However, it is worth mentioning that the mean difference between the scores of the two datasets is very low, at around 0.02 points.

3.2 | Temperature

Figure 9 shows the evolution in the monthly mean 2-m temperature over all the validation domain of CHAPTER (upscaled at 10 km), ERA5-Land, and E-OBS, for the whole period available in CHAPTER (i.e., 1981–2022). Whereas ERA5-Land presents a systematic positive bias

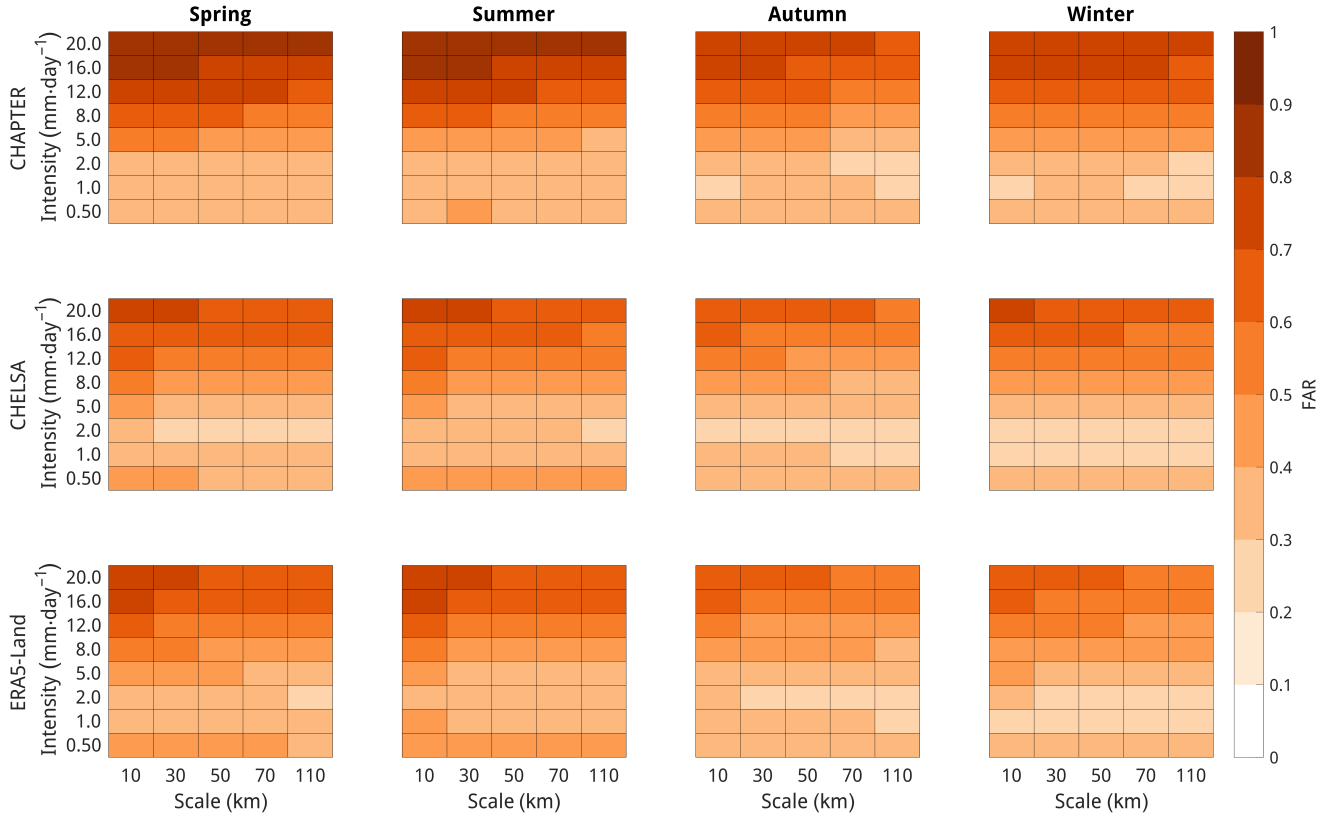

FIGURE 4 False alarm ratio (FAR) of the daily precipitation accumulation of CHAPTER (top) and CHELSA (center) at 10 km, and ERA5-Land (bottom) against E-OBS for the period 2003–2016. [Colour figure can be viewed at wileyonlinelibrary.com]

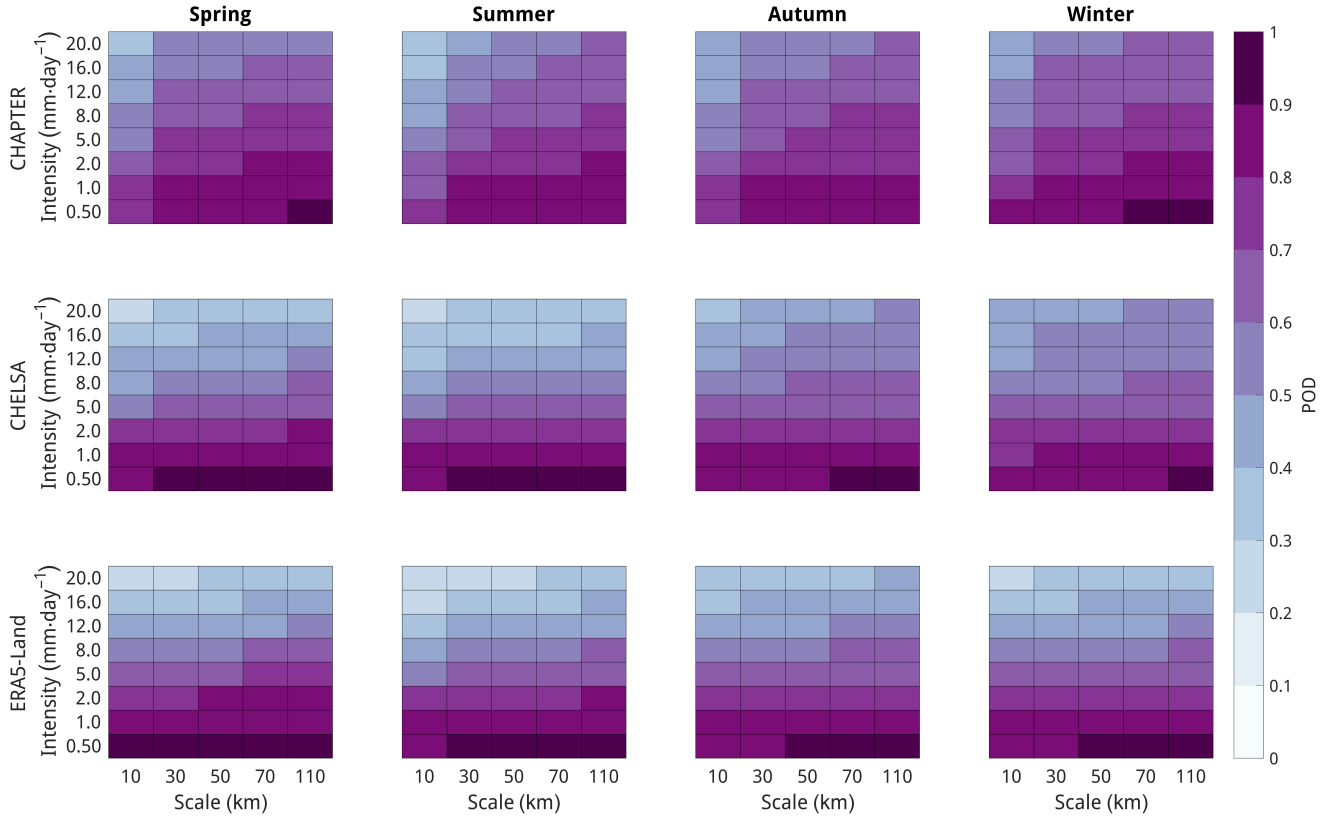

FIGURE 5 Probability of detection (POD) of the daily precipitation accumulation of CHAPTER (top) and CHELSA (center) at 10 km, and ERA5-Land (bottom) against E-OBS for the period 2003–2016. [Colour figure can be viewed at wileyonlinelibrary.com]

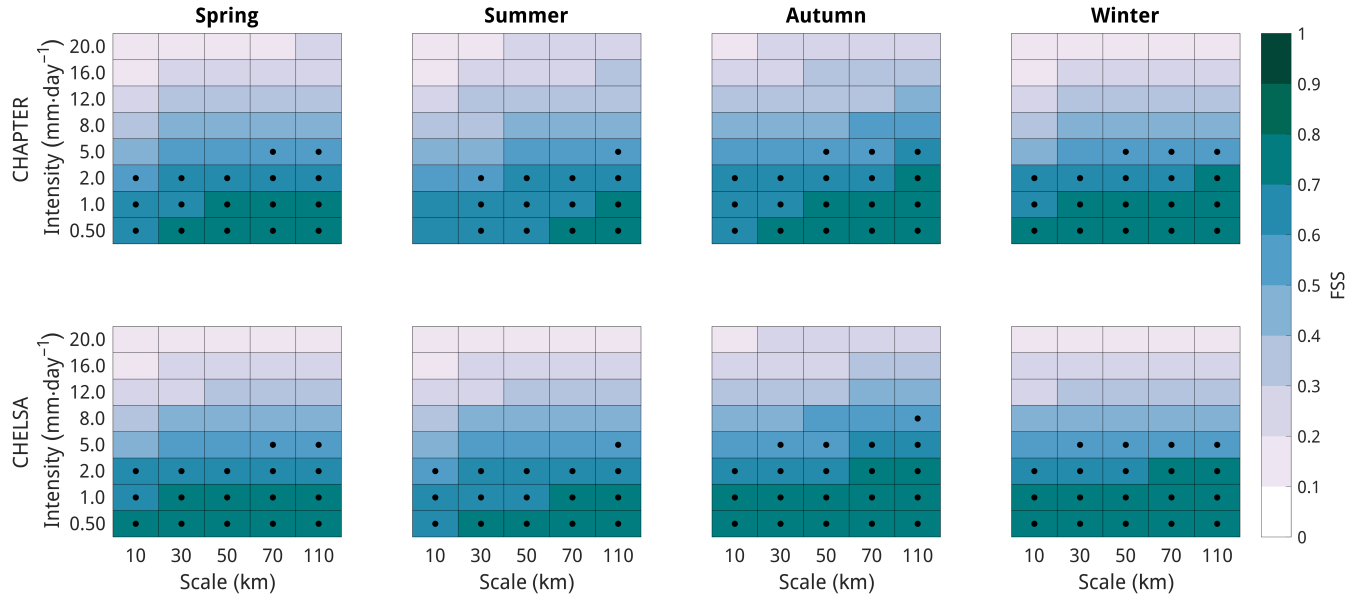

FIGURE 6 Fraction skill score (FSS) of the daily precipitation accumulation of CHAPTER (top) and CHELSA (bottom) against EURADCLIM for the period 2013–2016. All datasets are regridded on a regular grid of 3 km by 3 km. Black dots denote useful FSS values. [Colour figure can be viewed at wileyonlinelibrary.com]

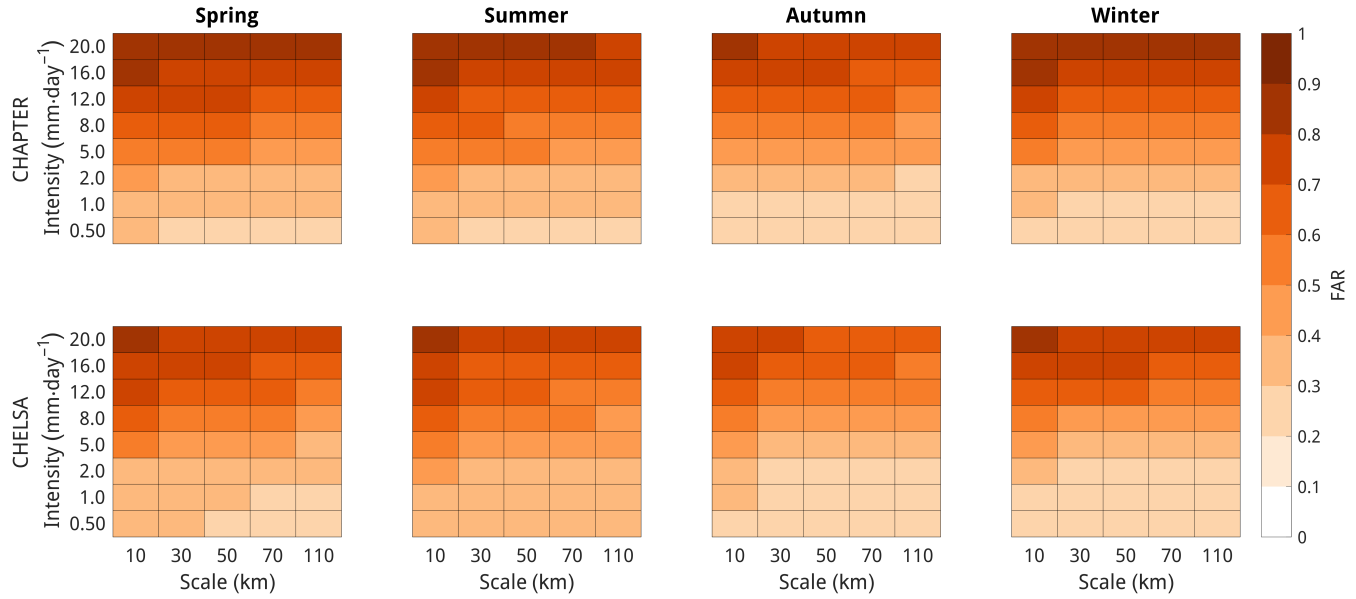

FIGURE 7 False alarm ratio (FAR) of the daily precipitation accumulation of CHAPTER (top) and CHELSA (bottom) against EURADCLIM for the period 2013–2016. All datasets are regridded on a regular grid of 3 km by 3 km. [Colour figure can be viewed at wileyonlinelibrary.com]

compared with E-OBS, CHAPTER seems to present a closer agreement with the observation dataset, with a slight negative bias starting after the year 1995 and a small positive bias before. Both datasets perfectly represent the evolution of the trends.

Table 1 presents the seasonal mean bias of temperature over all the domains, for the entire period. The positive bias in ERA5-Land mainly comes from the summer and autumn seasons, whereas CHAPTER presents the strongest negative bias in winter. CHAPTER has both a positive bias in summer and a negative bias in winter, whereas ERA5-Land has only a strong positive bias in summer, which could explain why doing the running mean (Figure 9) CHAPTER seems to have a closer agreement with the observations: the negative bias in winter compensates the positive one in summer.

Looking at the mean bias for each location (Figure 10), there is a clear overestimation of the temperature over the African coast. However, those large errors have perhaps more to do with the scarcity of data on this region than

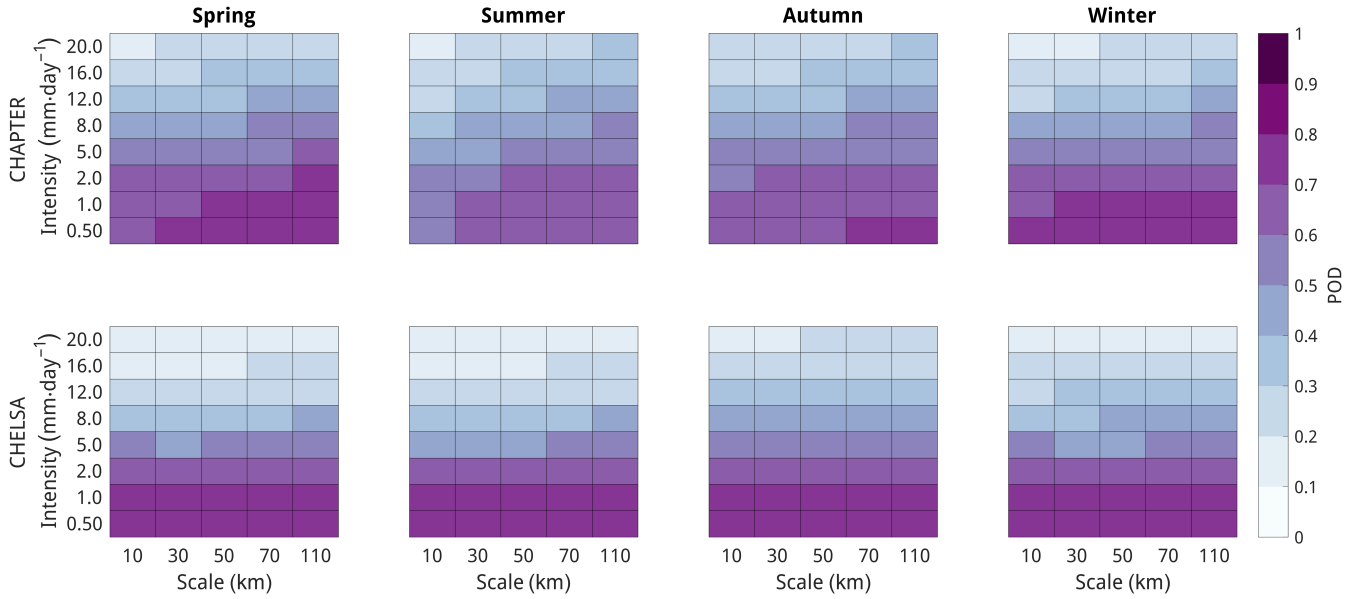

FIGURE 8 Probability of detection (POD) of the daily precipitation accumulation of CHAPTER (top) and CHELSA (bottom) against EURADCLIM for the period 2013–2016. All datasets are regridded on a regular grid of 3 km by 3 km. [Colour figure can be viewed at wileyonlinelibrary.com]

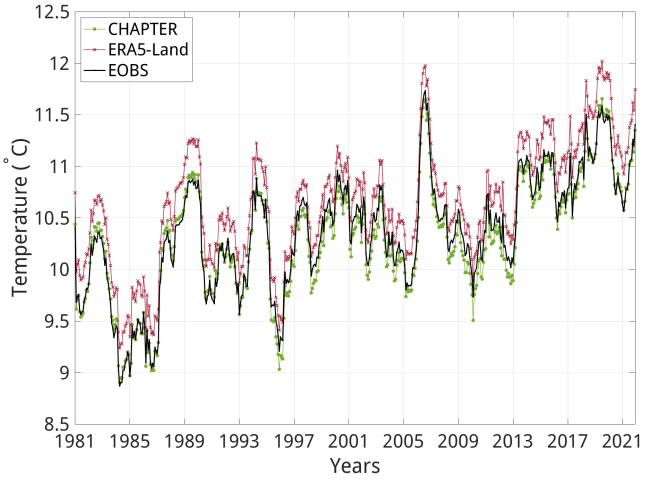

FIGURE 9 The 12-month running means of 2-m temperature between 1981 and 2022 for E-OBS (black straight line), ERA5-Land (red line with star markers), and CHAPTER (green dotted line). [Colour figure can be viewed at wileyonlinelibrary.com]

with the intrinsic deficiencies of the model. On another hand, the temperatures over the Alps are more frequently underestimated. It is important to note that, over these two regions, the same errors are observed both for CHAPTER and for ERA5-Land in both sign and magnitude.

Because of compensation, bias gives only partial information. The RMSE presented in Figure 11 accurately represents the average error's magnitude, though giving more weight to large errors. CHAPTER has generally higher RMSE than ERA5-Land does, with the highest mean RMSE of 2.18°C in winter (Table 2). This confirms that CHAPTER tends to have slightly higher differences with the temperatures of E-OBS but those differences compensate each other spatially and in time when computing the mean bias. On the other hand, ERA5-Land has a positive bias in summer only, creating a bigger difference with E-OBS when comparing the annual means. In terms of spatial analysis, we again find the largest errors over North Africa and the Alps.

3.3 | AV of CHAPTER over ERA5

The preceding subsections focus on comparing CHAPTER with state-of-the-art downscaling of ERA5: one statistical and one dynamic. This section directly contrasts CHAPTER with ERA5 to evaluate the AV of CHAPTER. Figure 12 illustrates the AV for temperature, where CHAPTER demonstrates a clear improvement. For nearly every grid cell across the domain and in all seasons, the AV is positive In the case of precipitation (Figure 13), positive AV are observed over the plains of central Europe during autumn, winter, and spring, whereas negative values occur in summer and over mountainous regions throughout all seasons. This indicates that during summer and in areas with complex orography, ERA5 aligns more closely with E-OBS.

The discrepancies between CHAPTER and E-OBS during summer or in specific regions may partly stem from E-OBS's inherent uncertainties, such as variable station density and measurement errors. As highlighted in Bandhauer *et al.* (2022), Pieri *et al.* (2015), and Isotta

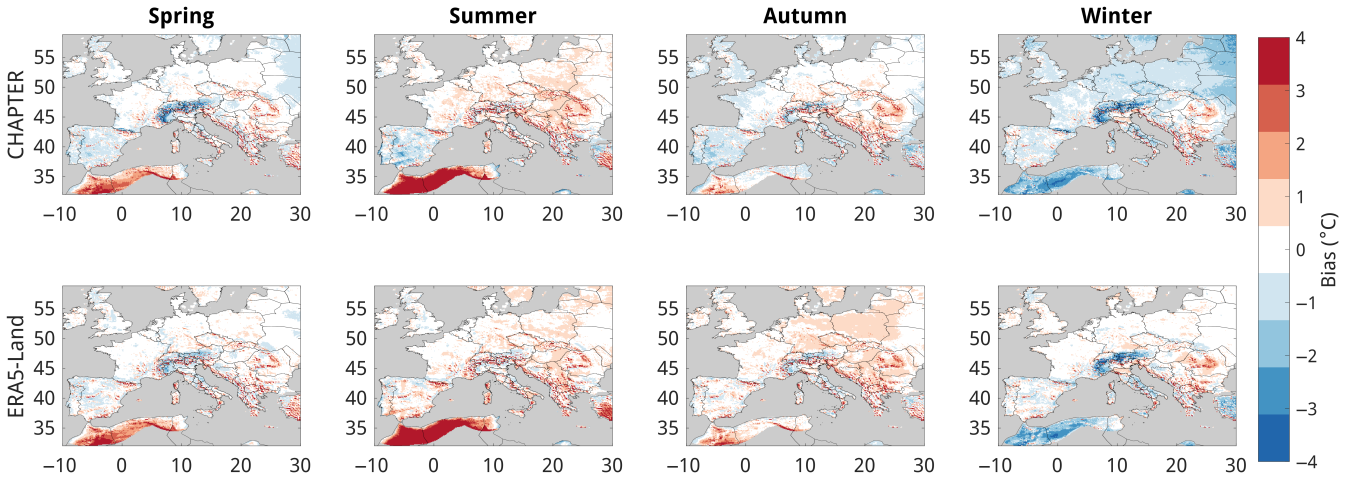

FIGURE 10 Bias of the daily mean temperature of CHAPTER (top) at 10 km and ERA5-Land (bottom) compared to E-OBS for the period 1981–2022. [Colour figure can be viewed at wileyonlinelibrary.com]

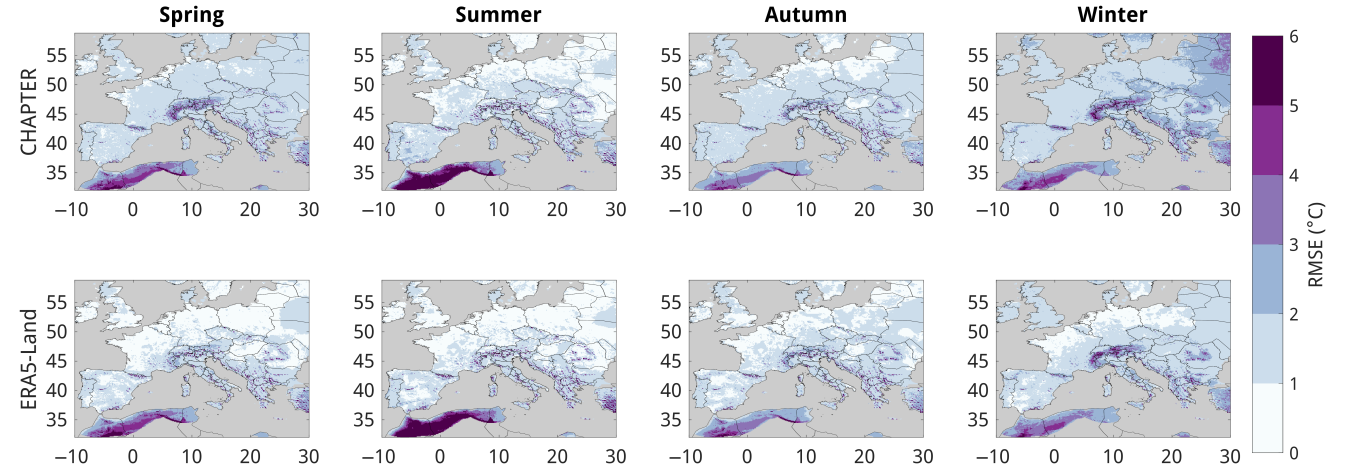

FIGURE 11 Root-mean-square error (RMSE) of the daily mean temperature of CHAPTER (top) at 10 km and ERA5-Land (bottom) compared with E-OBS for the period 1981–2022. [Colour figure can be viewed at wileyonlinelibrary.com]

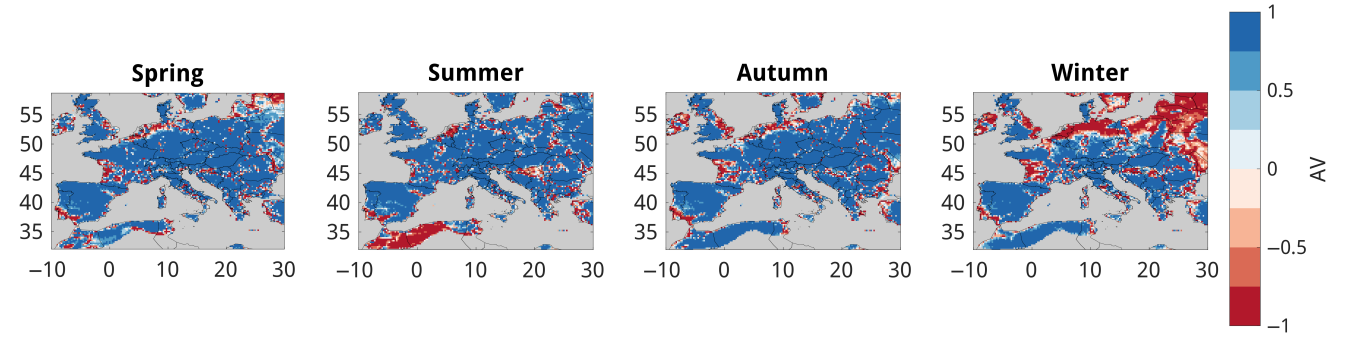

FIGURE 12 Added value (AV) for seasonal daily mean temperature (1981–2022) to assess the AV of CHAPTER over ERA5 when compared with E-OBS. [Colour figure can be viewed at wileyonlinelibrary.com]

et al. (2014), the sparse distribution of measurement stations in certain regions, particularly in high mountain areas, systematically underestimates extreme rainfall rates. Extreme precipitations are more frequently observed in summer, a season dominated by extreme convective precipitation events (Giorgi *et al.*, 2016; Llasat *et al.*, 2021).

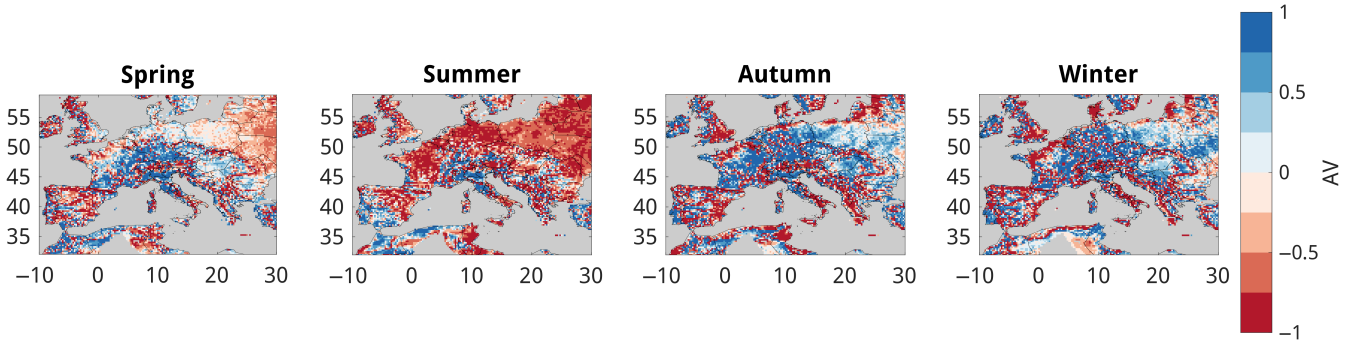

FIGURE 13 Added value (AV) for seasonal daily accumulated precipitation (1981–2022) to assess the AV of CHAPTER over ERA5 when compared with E-OBS. [Colour figure can be viewed at wileyonlinelibrary.com]

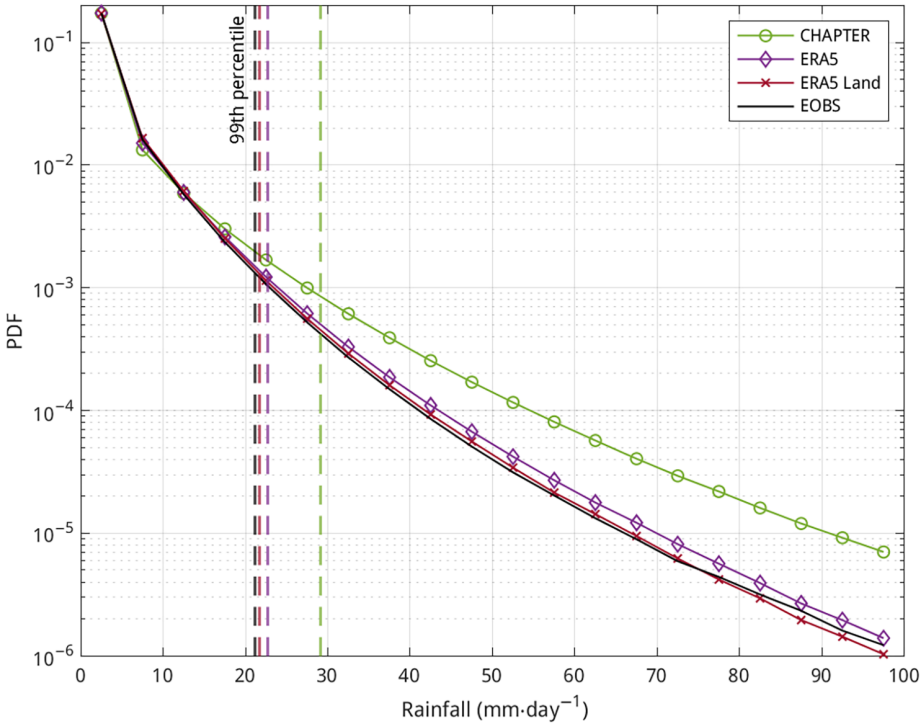

FIGURE 14 Probability density function (PDF) of the annual daily mean precipitation for the period 1981–2022 for the four datasets: E-OBS (straight black line), ERA5 (purple line with diamond markers), ERA5-Land (red line with cross markers), and CHAPTER (green dotted line). [Colour figure can be viewed at wileyonlinelibrary.com]

The ability of CHAPTER to capture intense rainfall events is further evidenced by the probability density function of the annual daily mean precipitation (Figure 14). The tail of CHAPTER's distribution extends significantly further than those of E-OBS or ERA5, with this divergence being most prominent in summer compared with other seasons (figure not shown).

The overestimation of extreme events by CHAPTER may not solely stem from its enhanced ability to represent convective events. An analysis of seasonal rainfall distributions (not shown) reveals that, in summer, CHAPTER overestimates extreme events compared with E-OBS, whereas ERA5 underestimates them. In winter, both CHAPTER and ERA5 overestimate intense rainfall compared with E-OBS. We hypothesize that ERA5 tends to overestimate large-scale precipitation intensity over Europe, as already found by Bandhauer *et al.* (2022), Lavers *et al.* (2022), and Rivoire *et al.* (2021). Consequently, CHAPTER overestimates intense rainfall in summer due to its superior resolution of convective events, and in winter because it is influenced by ERA5's bias in representing large-scale events. Overall, this leads to the annual overestimation shown in Figure 14. Further studies would be needed to validate this hypothesis.

4 | DISCUSSION AND CONCLUSIONS

The CHAPTER dataset, through its high-resolution dynamical downscaling of the ERA5 global reanalysis, offers a significant advancement in the realm of

climate and weather modeling for Europe and the Mediterranean basin. One of the primary benefits of CHAPTER is its cloud-resolving grid spacing at 3 km by 3 km, which allows for detailed and precise simulations of atmospheric phenomena along with hourly temporal resolution.

Compared with existing state-of-the-art datasets, CHAPTER matches their performance and presents an important AV by providing a rich list of three-dimensional variables, such as temperature, water vapor mass fraction, wind components including vertical velocity, and microphysical species mass fractions. This enhanced spatial resolution over such a long period, 42 years, is very valuable for comprehensive physical process studies and enables a deeper understanding of severe hydro-meteorological phenomena in a changing climate.

For instance, statistical analyses of lightning potential indices, maximum vertical velocities in updrafts, and hail statistics can be performed using CHAPTER data and be compared with observational data from recent climatologies (Punge & Kunz, 2016; Taszarek *et al.*, 2019). This will allow for a better understanding of the physics behind lightning and hailstorm phenomena and their predictability such as in Dowdy *et al.* (2020). Such insights are valuable for sectors like insurance, where risk assessment and damage prediction are critical.

Moreover, CHAPTER's high-resolution reanalysis fields, when coupled with models like the Continuum hydrological model (Silvestro *et al.*, 2013), could enable detailed studies of streamflow extremes and long-term water balances (Silvestro *et al.*, 2019). This is particularly important for regions with small hydrological catchments that are vulnerable to severe rainfall events (Alfieri *et al.*, 2015). By simulating various components of the water cycle, CHAPTER can produce indicators of meteorological, hydrological, and agricultural drought attributes, thus supporting decision-making in areas heavily affected by climate variability and extremes.

High-resolution reanalysis datasets like CHAPTER are also crucial for studying wildfires because they provide detailed and precise meteorological information that is essential for understanding and predicting fire behavior (Resco de Dios & Nolan, 2021). CHAPTER captures the fine-scale atmospheric conditions that influence wildfire dynamics, such as wind speed, humidity, and temperature variations but also, as already mentioned, lightning strikes (Müller *et al.*, 2020). Additionally, CHAPTER's comprehensive data can drive fire behavior models and inform forest management practices, ultimately contributing to more effective wildfire prevention and mitigation strategies like prescribed fires (Francos & Úbeda, 2021).

Despite its advantages, the CHAPTER dataset faces different challenges. First, the data for each day are produced by different independent runs that can create small discrepancies at 0000 UTC. This should not be a problem for the statistical application of CHAPTER described herein but needs to be evaluated when using CHAPTER to study the evolution of a specific event.

Second, the comparison with the ERA5-Land convection-parametrized downscaling does not show significant improvements across various metrics. This may be partly due to the pronounced double-penalty issue in high-resolution weather simulations. Such penalties arise from spatial discrepancies in the locations of heavy rainfall or temperature peaks, resulting in mismatches with observational data (Rossa *et al.*, 2008). This problem is intrinsic to simulations of deep moist convection, which are highly chaotic and difficult to predict with high accuracy. Though a fuzzy validation technique for precipitation addresses this issue to some extent, the most effective methods for enhancing precision involve the additional assimilation of radar observations (Lagasio *et al.*, 2019) or postprocessing reanalysis data using optimal interpolation techniques (Bonanno *et al.*, 2019).

Data assimilation is challenging to implement at the resolution provided by CHAPTER and on such a large territory (Pu, 2017). However, the integration of CHAPTER into multimodel ensemble-based approaches could mitigate this issue. Such approaches enhance the robustness of simulations and improve the representation of unresolved physics in convection-permitting models. Recent European efforts have shown that multimodel convection-permitting regional climate simulations provide a more realistic representation of heavy precipitation and improve confidence in simulating convection extremes (Ban *et al.*, 2021; Coppola *et al.*, 2020; Pichelli *et al.*, 2021).

Furthermore, CHAPTER's high-resolution reanalysis fields are poised to benefit machine-learning applications in weather and climate analysis. These applications can include data assimilation corrections (Farchi *et al.*, 2021) and improved parametrization of atmospheric processes in general circulation models, leveraging machine-learning methods to enhance predictive capabilities and model accuracy (Bochenek & Ustrnul, 2022).

The last point concerns CHAPTER uncertainties. ERA5 features an ensemble data assimilation component Isaksen *et al.* (2010) including one control and nine perturbed members. This ensemble provides background error estimates, enabling the estimation of analysis and short-range forecast uncertainties. In contrast, CHAPTER lacks an ensemble component that precludes a direct estimation of uncertainties analogous to those provided by the ensemble data assimilation systems of ERA5.

Nevertheless, several potential methods could be explored to assess the uncertainty in CHAPTER.

Since CHAPTER is a deterministic downscaling of ERA5, the 10-member ensemble of ERA5 could theoretically be used to generate 10 realizations of CHAPTER. The uncertainty could then be derived from the spread (e.g., maximum minus minimum values) across these realizations. Another approach involves generating a multiphysics ensemble by running CHAPTER with different parametrization schemes while keeping the deterministic ERA5 boundaries fixed. This method would provide insights into the sensitivity of CHAPTER's outputs to model physics. However, these approaches would require performing the CHAPTER downscaling for each ensemble member or for each set of parametrizations tested, which is computationally prohibitive.

A more feasible alternative is the application of a pragmatic, low-budget postprocessing approach, as described by Theis *et al.* (2005). This methodology derives probabilistic forecasts from deterministic model outputs by examining the spatiotemporal neighborhood of a grid point to generate a set of forecasts. These forecasts are then used to calculate probabilistic metrics, such as ensemble mean and spread (e.g., maximum minus minimum values) for the central point. Applying this method to CHAPTER would allow the derivation of a spatiotemporal uncertainty metric at each grid point without the need for ensemble simulations or historical error statistics, making it a cost-effective solution.

Finally, we want to point out that fuzzy verification techniques provide insights into the spatial scales at which CHAPTER is reliable. As shown in the Section 2.2, CHAPTER reliability aligns with that of ERA5-Land and CHELSA, both of which are widely recognized as valuable downscaling products of ERA5. This alignment supports the credibility of CHAPTER's outputs at comparable spatial scales.

Overall, CHAPTER can be a valuable resource for climate scientists, meteorologists, and stakeholders involved in risk assessment and mitigation of extreme weather events. It offers critical insights and a robust foundation for future research and applications aimed at understanding and managing weather-related hazards in the context of global warming.

ACKNOWLEDGEMENTS

We gratefully acknowledge the Gauss Centre for Supercomputing e.V. (www.gauss-centre.eu) for supporting this project by providing computing time on the GCS Supercomputer SuperMUC-NG at Leibniz Supercomputing Centre (www.lrz.de). Parts of the development of the data-publication methodology behind the LRZ FAIR data portal have been supported by the project InHPC-DE, funded by the German Federal Ministry of Education and Research (Förderkennzeichen 16HPC02).

Additionally, the research activities described in this article have been partially funded by the Italian program "Piano Nazionale di Ripresa e Resilienza-PNRR", Missione 4 Componente 2, Investimento 3.3-D.M.352 09/04/2022, M.U.R., Ministry of University and Research.

This research has also been partially supported by the projects I-CHANGE (Individual Change of Habits Needed for Green European transition; https://cordis.europa.eu/project/id/101037193) and TRIGGER (Solutions for Mitigating Climate-induced Health Threats; https://cordis.europa.eu/project/id/101057739).

Finally, we sincerely thank Professor C. Pasquero from the University Milano-Bicocca for her precious support through various and stimulating exchanges, as well as for her parallel work on the CHAPTER dataset, which has greatly enriched our research. Open access publishing facilitated by Universita degli Studi di Genova, as part of the Wiley - CRUI-CARE agreement.

CONFLICT OF INTEREST STATEMENT

The authors declare no conflict of interest.

DATA AVAILABILITY STATEMENT

The data that support the findings of this study are openly available in Leibniz Supercomputing Centre, LRZ at https://rdm.lab.lrz.de/records/0ppk7-znk14, reference number 10.25927/0ppk7-znk14.

A first release of selected variables from CHAPTER has been made available on the FAIR data portal of LRZ (Leibniz Supercomputing Centre, LRZ, Germany) through the GLOBUS Online file-transfer service. The dataset description and download instructions are reachable through the following Digital Object Identifier for the dataset: https://doi.org/10.25927/0ppk7-znk14 (Tartaglione *et al.*, 2024). The data are also accessible anonymously and directly through the repertory at https://chapter.rdm.lab.lrz.de/.

For now, the following data are available within the dataset: hourly cumulated precipitation ("PREC_AC_NC", in mm), zonal and meridional component of wind at 10 m ("U10" and "V10", in $m \cdot s^{-1}$), temperature at 2 m ("T2", in K), specific humidity at 2 m ("Q2", in $kg \cdot kg^{-1}$), hourly cumulated snow ("SNOW_ACC_NC", in meters of water equivalent), downward short-wave radiation at the bottom ("SWDNB", in $W \cdot m^{-2}$), downward long-wave radiation at the bottom ("LWDNB", in $W \cdot m^{-2}$), upward long-wave radiation at the bottom ("LWUPB", in $W \cdot m^{-2}$).

The data have been released under a CC-BY 4.0 license (i.e., free usage, but requiring attribution/credits to the source). Further releases of vertical variables are envisaged.

ORCID

Lisa Bernini https://orcid.org/0009-0008-8730-8636
Martina Lagasio https://orcid.org/0000-0002-2468-3577

REFERENCES

Alfieri, L., Burek, P., Feyen, L. & Forzieri, G. (2015) Global warming increases the frequency of river floods in Europe. *Hydrology and Earth System Sciences*, 19(5), 2247–2260.

Apicella, L., Puca, S., Lagasio, M., Meroni, A., Milelli, M., Vela, N. et al. (2021) The predictive capacity of the high resolution weather research and forecasting model: a year-long verification over Italy. *Bulletin of Atmospheric Science and Technology*, 2(1), 3.

Bakkensen, L.A. (2017) Mediterranean hurricanes and associated damage estimates. *Journal of Extreme Events*, 4(2), 1750008.

Ban, N., Caillaud, C., Coppola, E., Pichelli, E., Sobolowski, S., Adinolfi, M. et al. (2021) The first multi-model ensemble of regional climate simulations at kilometer-scale resolution, part I: evaluation of precipitation. *Climate Dynamics*, 57, 275–302.

Bandhauer, M., Isotta, F., Lakatos, M., Lussana, C., Båserud, L., Izsák, B. et al. (2022) Evaluation of daily precipitation analyses in E-OBS (v19. 0e) and ERA5 by comparison to regional high-resolution datasets in European regions. *International Journal of Climatology*, 42(2), 727–747.

Bochenek, B. & Ustrnul, Z. (2022) Machine learning in weather prediction and climate analyses—applications and perspectives. *Atmosphere*, 13(2), 180.

Bollmeyer, C., Keller, J., Ohlwein, C., Wahl, S., Crewell, S., Friederichs, P. et al. (2015) Towards a high-resolution regional reanalysis for the European CORDEX domain. *Quarterly Journal of the Royal Meteorological Society*, 141(686), 1–15.

Bonanno, R., Lacavalla, M. & Sperati, S. (2019) A new high-resolution meteorological reanalysis Italian dataset: MERIDA. *Quarterly Journal of the Royal Meteorological Society*, 145(721), 1756–1779.

Calleja-Agius, J., England, K. & Calleja, N. (2021) The effect of global warming on mortality. *Early Human Development*, 155, 105222.

Canadell, J.G., Monteiro, P.M.S., Costa, M.H., Cotrim da Cunha, L., Cox, P.M., Eliseev, A.V. et al. (2021) *Global carbon and other biogeochemical cycles and feedbacks Cambridge*, Vol. 12. United Kingdom and New York, NY: Cambridge University Press, pp. 673–816.

Cerenzia, I.M.L., Giordani, A., Paccagnella, T. & Montani, A. (2022) Towards a convection-permitting regional reanalysis over the Italian domain. *Meteorological Applications*, 29(5), e2092.

Coppola, E., Sobolowski, S., Pichelli, E., Raffaele, F., Ahrens, B., Anders, I. et al. (2020) A first-of-its-kind multi-model convection permitting ensemble for investigating convective phenomena over Europe and the Mediterranean. *Climate Dynamics*, 55, 3–34.

Cornes, R.C., van der Schrier, G., van den Besselaar, E.J. & Jones, P.D. (2018) An ensemble version of the E-OBS temperature and precipitation data sets. *Journal of Geophysical Research: Atmospheres*, 123(17), 9391–9409.

Cramer, W., Guiot, J., Fader, M., Garrabou, J., Gattuso, J.P., Iglesias, A. et al. (2018) Climate change and interconnected risks to sustainable development in the Mediterranean. *Nature Climate Change*, 8(11), 972–980.

Dahlgren, P., Landelius, T., Kållberg, P. & Gollvik, S. (2016) A high-resolution regional reanalysis for Europe. Part 1: three-dimensional reanalysis with the regional HIgh-resolution limited-area model (HIRLAM). *Quarterly Journal of the Royal Meteorological Society*, 142(698), 2119–2131.

Dalla Torre, D., Di Marco, N., Menapace, A., Avesani, D., Righetti, M. & Majone, B. (2024) Suitability of ERA5-land reanalysis dataset for hydrological modelling in the alpine region. *Journal of Hydrology: Regional Studies*, 52, 101718.

Diffenbaugh, N.S., Singh, D., Mankin, J.S., Horton, D.E., Swain, D.L., Touma, D. et al. (2017) Quantifying the influence of global warming on unprecedented extreme climate events. *Proceedings of the National Academy of Sciences*, 114(19), 4881–4886.

Dosio, A., Panitz, H.J., Schubert-Frisius, M. & Lüthi, D. (2015) Dynamical downscaling of CMIP5 global circulation models over CORDEX-Africa with COSMO-CLM: evaluation over the present climate and analysis of the added value. *Climate Dynamics*, 44, 2637–2661.

Dowdy, A.J., Soderholm, J., Brook, J., Brown, A. & McGowan, H. (2020) Quantifying hail and lightning risk factors using long-term observations around Australia. *Journal of Geophysical Research: Atmospheres*, 125(21), 2020JD033101.

Ebert, E.E. (2008) Fuzzy verification of high-resolution gridded forecasts: a review and proposed framework. *Meteorological Applications: A Journal of Forecasting, Practical Applications, Training Techniques and Modelling*, 15(1), 51–64.

Efron, B. (1992) Bootstrap methods: another look at the Jackknife. In: *Breakthroughs in statistics: methodology and distribution*. New York, NY: Springer, pp. 569–593.

Farchi, A., Laloyaux, P., Bonavita, M. & Bocquet, M. (2021) Using machine learning to correct model error in data assimilation and forecast applications. *Quarterly Journal of the Royal Meteorological Society*, 147(739), 3067–3084.

Fiori, E., Ferraris, L., Molini, L., Siccardi, F., Kranzlmueller, D. & Parodi, A. (2017) Triggering and evolution of a deep convective system in the Mediterranean Sea: modelling and observations at a very fine scale. *Quarterly Journal of the Royal Meteorological Society*, 143(703), 927–941.

Francos, M. & Úbeda, X. (2021) Prescribed fire management. *Current Opinion in Environmental Science & Health*, 21, 100250.

Giordani, A., Cerenzia, I.M.L., Paccagnella, T. & Di Sabatino, S. (2023) SPHERA, a new convection-permitting regional reanalysis over Italy: improving the description of heavy rainfall. *Quarterly Journal of the Royal Meteorological Society*, 149(752), 781–808.

Giorgi, F., Torma, C., Coppola, E., Ban, N., Schär, C. & Somot, S. (2016) Enhanced summer convective rainfall at alpine high elevations in response to climate warming. *Nature Geoscience*, 9(8), 584–589.

Gleeson, E., Whelan, E. & Hanley, J. (2017) Met Éireann high resolution reanalysis for Ireland. *Advances in Science and Research*, 14, 49–61.

Grillakis, M.G. (2019) Increase in severe and extreme soil moisture droughts for Europe under climate change. *Science of the Total Environment*, 660, 1245–1255.

Han, J. & Pan, H.L. (2011) Revision of convection and vertical diffusion schemes in the NCEP global forecast system. *Weather and Forecasting*, 26(4), 520–533.

von Hardenberg, J., Parodi, A., Pieri, A.B. & Provenzale, A. (2015) Impact of microphysics and convective parameterizations on dynamical downscaling for the European domain. In: *Engineering geology for society and territory-volume 1: climate change and*

engineering geology. Cham, Switzerland: Springer International Publishing, pp. 209–213.

Hendry, A., Haigh, I.D., Nicholls, R.J., Winter, H., Neal, R., Wahl, T. et al. (2019) Assessing the characteristics and drivers of compound flooding events around the UK coast. *Hydrology and Earth System Sciences*, 23(7), 3117–3139.

Hersbach, H., Bell, B., Berrisford, P., Hirahara, S., Horányi, A., Muñoz-Sabater, J. et al. (2020) The ERA5 global reanalysis. *Quarterly Journal of the Royal Meteorological Society*, 146(730), 1999–2049.

Hofstra, N., Haylock, M., New, M. & Jones, P.D. (2009) Testing E-OBS European high-resolution gridded data set of daily precipitation and surface temperature. *Journal of Geophysical Research: Atmospheres*, 114(D21), D2101.1–D2101.16.

Hong, S.Y., Noh, Y. & Dudhia, J. (2006) A new vertical diffusion package with an explicit treatment of entrainment processes. *Monthly Weather Review*, 134(9), 2318–2341.

Hosseinzadehtalaei, P., Tabari, H. & Willems, P. (2020) Climate change impact on short-duration extreme precipitation and intensity–duration–frequency curves over Europe. *Journal of Hydrology*, 590, 125249.

Iacono, M.J., Mlawer, E.J., Clough, S.A. & Morcrette, J.J. (2000) Impact of an improved longwave radiation model, RRTM, on the energy budget and thermodynamic properties of the NCAR community climate model, CCM3. *Journal of Geophysical Research: Atmospheres*, 105(D11), 14873–14890.

Iacono, M.J., Delamere, J.S., Mlawer, E.J., Shephard, M.W., Clough, S.A. & Collins, W.D. (2008) Radiative forcing by long-lived greenhouse gases: calculations with the AER radiative transfer models. *Journal of Geophysical Research: Atmospheres*, 113(D13), D13103.1–D13103.8.

Isaksen, L., Bonavita, M., Buizza, R., Fisher, M., Haseler, J., Leutbecher, M. et al. (2010) Ensemble of data assimilations at ECMWF. *ECMWF Technical Memoranda*, 636, 1–48.

Isotta, F.A., Frei, C., Weilguni, V., Percec Tadic, M., Lassegues, P., Rudolf, B. et al. (2014) The climate of daily precipitation in the Alps: development and analysis of a high-resolution grid dataset from pan-alpine rain-gauge data. *International Journal of Climatology*, 34(5), 1657–1675.

Karger, D.N., Wilson, A.M., Mahony, C., Zimmermann, N.E. & Jetz, W. (2021) Global daily 1 km land surface precipitation based on cloud cover-informed downscaling. *Scientific Data*, 8(1), 307.

Karki, R., Gerlitz, L., Schickhoff, U., Scholten, T., Böhner, J. et al. (2017) Quantifying the added value of convection-permitting climate simulations in complex terrain: a systematic evaluation of WRF over the Himalayas. *Earth System Dynamics*, 8(3), 507–528.

Kendon, E., Prein, A., Senior, C. & Stirling, A. (2021) Challenges and outlook for convection-permitting climate modelling. *Philosophical Transactions of the Royal Society A*, 379(2195), 20190547.

Lagasio, M., Parodi, A., Pulvirenti, L., Meroni, A.N., Boni, G., Pierdicca, N. et al. (2019) A synergistic use of a high-resolution numerical weather prediction model and high-resolution earth observation products to improve precipitation forecast. *Remote Sensing*, 11(20), 2387.

Lavers, D.A., Simmons, A., Vamborg, F. & Rodwell, M.J. (2022) An evaluation of ERA5 precipitation for climate monitoring. *Quarterly Journal of the Royal Meteorological Society*, 148(748), 3152–3165.

Llasat, M.C., del Moral, A., Cortès, M. & Rigo, T. (2021) Convective precipitation trends in the Spanish Mediterranean region. *Atmospheric Research*, 257, 105581.

Lucas-Picher, P., Argüeso, D., Brisson, E., Tramblay, Y., Berg, P., Lemonsu, A. et al. (2021) Convection-permitting modeling with regional climate models: latest developments and next steps. *Wiley Interdisciplinary Reviews: Climate Change*, 12(6), e731.

Menne, M.J., Durre, I., Vose, R.S., Gleason, B.E. & Houston, T.G. (2012) An overview of the global historical climatology network-daily database. *Journal of Atmospheric and Oceanic Technology*, 29(7), 897–910.

Mlawer, E.J., Taubman, S.J., Brown, P.D., Iacono, M.J. & Clough, S.A. (1997) Radiative transfer for inhomogeneous atmospheres: RRTM, a validated correlated-k model for the longwave. *Journal of Geophysical Research: Atmospheres*, 102(D14), 16663–16682.

Moriondo, M., Good, P., Durao, R., Bindi, M., Giannakopoulos, C. & Corte-Real, J. (2006) Potential impact of climate change on fire risk in the Mediterranean area. *Climate Research*, 31(1), 85–95.

Müller, M.M., Vilà-Vilardell, L. & Vacik, H. (2020) Towards an integrated forest fire danger assessment system for the European Alps. *Ecological Informatics*, 60, 101151.

Muñoz-Sabater, J., Dutra, E., Agustí-Panareda, A., Albergel, C., Arduini, G., Balsamo, G. et al. (2021) ERA5-land: a state-of-the-art global reanalysis dataset for land applications. *Earth System Science Data*, 13(9), 4349–4383.

Ntagkounakis, G.E., Nastos, P.T. & Kapsomenakis, Y. (2023) Statistical downscaling of ERA5 reanalysis precipitation over the complex terrain of Greece. *Environmental Sciences Proceedings*, 26(1), 81.

Overeem, A., van den Besselaar, E., van der Schrier, G., Meirink, J.F., van der Plas, E. & Leijnse, H. (2022) EURADCLIM: the European climatological high-resolution gauge-adjusted radar precipitation dataset. *Earth System Science Data Discussions*, 2022, 1–34.

Pan, H. (1995) Implementing a mass flux convection parameterization package for the NCEP medium-range forecast model. *NMC Office Note*, 409, 1–43.

Pichelli, E., Coppola, E., Sobolowski, S., Ban, N., Giorgi, F., Stocchi, P. et al. (2021) The first multi-model ensemble of regional climate simulations at kilometer-scale resolution part 2: historical and future simulations of precipitation. *Climate Dynamics*, 56, 3581–3602.

Pieri, A.B., von Hardenberg, J., Parodi, A. & Provenzale, A. (2015) Sensitivity of precipitation statistics to resolution, microphysics, and convective parameterization: a case study with the high-resolution WRF climate model over Europe. *Journal of Hydrometeorology*, 16(4), 1857–1872.

Prein, A.F., Langhans, W., Fosser, G., Ferrone, A., Ban, N., Goergen, K. et al. (2015) A review on regional convection-permitting climate modeling: demonstrations, prospects, and challenges. *Reviews of Geophysics*, 53(2), 323–361.

Pu, Z. (2017) Surface data assimilation and near-surface weather prediction over complex terrain. In: *Data assimilation for atmospheric, oceanic and hydrologic applications*, Vol. III. Cham, Switzerland: Springer International Publishing, pp. 219–240.

Punge, H.J. & Kunz, M. (2016) Hail observations and hailstorm characteristics in Europe: a review. *Atmospheric Research*, 176, 159–184.

Raffa, M., Reder, A., Marras, G.F., Mancini, M., Scipione, G., Santini, M. et al. (2021) VHR-REA_IT dataset: very high resolution dynamical downscaling of ERA5 reanalysis over Italy by COSMO-CLM. *Data*, 6(8), 88.

Rahmstorf, S. & Coumou, D. (2011) Increase of extreme events in a warming world. *Proceedings of the National Academy of Sciences*, 108(44), 17905–17909.

Reder, A., Raffa, M., Padulano, R., Rianna, G. & Mercogliano, P. (2022) Characterizing extreme values of precipitation at very high resolution: an experiment over twenty European cities. *Weather and Climate Extremes*, 35, 100407.

Resco de Dios, V. & Nolan, R.H. (2021) Some challenges for forest fire risk predictions in the21st century. *Forests*, 12(4), 469.

Ridal, M., Bazile, E., Le Moigne, P., Randriamampianina, R., Schimanke, S., Andrae, U. et al. (2024) CERRA, the Copernicus European regional reanalysis system. *Quarterly Journal of the Royal Meteorological Society*, 150(763), 3385–3411.

Rivoire, P., Martius, O. & Naveau, P. (2021) A comparison of moderate and extreme ERA-5 daily precipitation with two observational data sets. Earth and space. *Science*, 8(4), e2020EA001633.

Roberts, N.M. & Lean, H.W. (2008) Scale-selective verification of rainfall accumulations from high-resolution forecasts of convective events. *Monthly Weather Review*, 136(1), 78–97.

Rossa, A., Nurmi, P. & Ebert, E. (2008) Overview of methods for the verification of quantitative precipitation forecasts. In: *Precipitation: advances in measurement, estimation and prediction*. Berlin, Heidelberg: Springer Berlin Heidelberg, pp. 419–452.

Rossa, A., Liechti, K., Zappa, M., Bruen, M., Germann, U., Haase, G. et al. (2011) The COST 731 action: a review on uncertainty propagation in advanced hydro-meteorological forecast systems. *Atmospheric Research*, 100(2–3), 150–167.

Schär, C., Vidale, P.L., Lüthi, D., Frei, C., Häberli, C., Liniger, M.A. et al. (2004) The role of increasing temperature variability in European summer heatwaves. *Nature*, 427(6972), 332–336.

Schimanke, S., Ridal, M., Le Moigne, P., Berggren, L., Undén, P., Randriamampianina, R. et al. (2021) CERRA sub-daily regional reanalysis data for Europe on single levels from 1984 to present. Copernicus Climate Change Service (C3S) Climate Data Store (CDS).

Silvestro, F., Gabellani, S., Delogu, F., Rudari, R. & Boni, G. (2013) Exploiting remote sensing land surface temperature in distributed hydrological modelling: the example of the continuum model. *Hydrology and Earth System Sciences*, 17(1), 39–62.

Silvestro, F., Rossi, L., Campo, L., Parodi, A., Fiori, E., Rudari, R. et al. (2019) Impact-based flash-flood forecasting system: sensitivity to high resolution numerical weather prediction systems and soil moisture. *Journal of Hydrology*, 572, 388–402.

Skamarock, W.C., Klemp, J.B., Dudhia, J., Gill, D.O., Barker, D.M., Duda, M.G. et al. (2008) A description of the advanced research WRF version 3. *NCAR Technical Note*, 475, 113.

Smirnova, T.G., Brown, J.M. & Benjamin, S.G. (1997) Performance of different soil model configurations in simulating ground surface temperature and surface fluxes. *Monthly Weather Review*, 125(8), 1870–1884.

Smirnova, T.G., Brown, J.M., Benjamin, S.G. & Kim, D. (2000) Parameterization of cold-season processes in the MAPS land-surface scheme. *Journal of Geophysical Research: Atmospheres*, 105(D3), 4077–4086.

Tartaglione, N., Paordi, A., Bernini, L., Hachinger, S. & Kranzlmüller, D. (2024) CHAPTER: 3 × 3 km meteorological data 1981–2022 for Europe: 2D extracted fields. *GLOBUS, [Data Set]*. Available from: https://doi.org/10.25927/0ppk7-znk14

Taszarek, M., Allen, J., Púčik, T., Groenemeijer, P., Czernecki, B., Kolendowicz, L. et al. (2019) A climatology of thunderstorms across Europe from a synthesis of multiple data sources. *Journal of Climate*, 32(6), 1813–1837.

Theis, S., Hense, A. & Damrath, U. (2005) Probabilistic precipitation forecasts from a deterministic model: a pragmatic approach. *Meteorological Applications*, 12(3), 257–268.

Trenberth, K.E., Koike, T. & Onogi, K. (2008) Progress and prospects for reanalysis for weather and climate. *Eos, Transactions American Geophysical Union*, 89(26), 234–235.

Vannucchi, V., Taddei, S., Capecchi, V., Bendoni, M. & Brandini, C. (2021) Dynamical downscaling of era5 data on the north-western mediterranean sea: from atmosphere to high-resolution coastal wave climate. *Journal of Marine Science and Engineering*, 9(2), 208.

Vautard, R., Gobiet, A., Sobolowski, S., Kjellström, E., Stegehuis, A., Watkiss, P. et al. (2014) The European climate under a 2 C global warming. *Environmental Research Letters*, 9(3), 034006.

Vié, B., Molinié, G., Nuissier, O., Vincendon, B., Ducrocq, V., Bouttier, F. et al. (2012) Hydro-meteorological evaluation of a convection-permitting ensemble prediction system for Mediterranean heavy precipitating events. *Natural Hazards and Earth System Sciences*, 12(8), 2631–2645.

Wahl, S., Bollmeyer, C., Crewell, S., Figura, C., Friederichs, P., Hense, A. et al. (2017) A novel convective-scale regional reanalysis COSMO-REA2: improving the representation of precipitation. *Meteorologische Zeitschrift*, 26(4), 345–361.

Warrach-Sagi, K., Schwitalla, T., Wulfmeyer, V. & Bauer, H.S. (2013) Evaluation of a climate simulation in Europe based on the WRF–NOAH model system: precipitation in Germany. *Climate Dynamics*, 41, 755–774.

Weilnhammer, V., Schmid, J., Mittermeier, I., Schreiber, F., Jiang, L., Pastuhovic, V. et al. (2021) Extreme weather events in europe and their health consequences–a systematic review. *International Journal of Hygiene and Environmental Health*, 233, 113688.

Wu, X., Su, J., Ren, W., Lü, H. & Yuan, F. (2023) Statistical comparison and hydrological utility evaluation of ERA5-land and IMERG precipitation products on the Tibetan Plateau. *Journal of Hydrology*, 620, 129384.

How to cite this article: Bernini, L., Lagasio, M., Milelli, M., Oberto, E., Parodi, A., Hachinger, S. *et al.* (2025) Convection-permitting dynamical downscaling of ERA5 for Europe and the Mediterranean basin. *Quarterly Journal of the Royal Meteorological Society*, e5014. Available from: https://doi.org/10.1002/qj.5014